Stability of microturbulent drift modes during internal transport barrier formation in the Alcator C-Mod radio frequency heated H-mode

M. H. Redi

Princeton Plasma Physics Laboratory, Princeton, NJ 08540, USA

C. L. Fiore

Plasma Science and Fusion Center, MIT, Cambridge, MA 02139, USA

W. Dorland

Institute for Plasma Research, U. MD, College Park, MD 20742, USA

D. R. Mikkelsen, G. Rewoldt

Princeton Plasma Physics Laboratory, Princeton, NJ 08540, USA

P. T. Bonoli, D. R. Ernst, J. E. Rice, S. J. Wukitch

Plasma Science and Fusion Center, MIT, Cambridge, MA 02139, USA

(Received

Recent H-mode experiments on Alcator C-Mod [I. H. Hutchinson, *et al.*, Phys. Plas. **1**, 1511 (1994)] which exhibit an internal transport barrier (ITB), have been examined with flux tube geometry gyrokinetic simulations, using the massively parallel code GS2 [M. Kotschenreuther, G. Rewoldt, and W. M. Tang, Comput. Phys. Commun. **88**, 128 (1995)]. The simulations support the picture of ion/electron temperature gradient (ITG/ETG) microturbulence driving high η_i/η_e and that stable ITG correlates with reduced particle transport and improved η_i on C-Mod. Nonlinear calculations for C-Mod confirm initial linear simulations, which predicted ITG stability in the barrier region just before ITB formation, without invoking $\boldsymbol{E}\times\boldsymbol{B}$ shear suppression of turbulence. Nonlinear fluxes are in agreement with experimental analysis within

error bars. Heat transport coefficients χ_e and χ_i agree with experimental analysis within a factor of two in the plasma core. Better diagnostic measurements and more extensive nonlinear simulations are still needed for comprehensive validation of the microturbulence simulation model.

(PACS numbers: 52.30.Gz, 52.35.Ra, 52.55.Fa)

I. INTRODUCTION

Recent years have seen exciting and dramatic progress in the development and application of computational physics methods for predicting drift wave microturbulence and transport in magnetically confined plasma experiments as may be seen in the papers surveyed in the reviews by Horton[1], Tang[2] and Terry[3] and in the conference summary by Itoh[4]. Validation of gyrokinetic-based models of drift wave turbulence is being sought *via* comparative simulations of high performance plasma experiments for new understanding of transport. These massively parallel, nonlinear, fully electromagnetic, nonadiabatic, gyrokinetic calculations are in the initial stages of application toward experimentally validated, global, nonlocal, first principles calculations of plasma transport.

When internal barriers to plasma particle and energy transport develop, high energy plasma is well confined, a necessary step toward economical fusion reactors. In this paper plasma conditions, just before an internal transport barrier (ITB) is established on Alcator C-Mod[5], are analysed using the GS2[6,7] gyrokinetic code. Because C-Mod is a toroidal magnetic confinement device with high toroidal field, high plasma density, and radio frequency (RF) heating, its transport characteristics are of special interest, being relevant to fusion reactor scenarios[8]. The linear[9] and nonlinear[10] simulations predict, just before ITB formation (at the "trigger time"), that plasma drift wave turbulence is suppressed in the plasma core, is quiescent where the ITB will form, and of classic ion temperature gradient character outside this region. Unlike ITBs on other magnetically confined fusion devices, this ITB is found to occur without either weak or reversed magnetic shear, and without strong plasma velocity shear[11-13], the source of the usual ***ExB*** shear suppression of linear drift wave turbulence[14-16].

We describe the experiment and physics analysis in Sec. II and in Sec. III give a discussion of the gyrokinetic equations. In Sec. IV are found details of the simulation parameters and results of the microstability analysis, along with a comparison of simulated fluxes to those from transport analysis. A summary and conclusions are given in Sec. V.

II. THE EXPERIMENT: INTERNAL TRANSPORT BARRIER IN ALCATOR C-MOD RF H-MODE

Following off-axis RF heating and establishment of an H-mode, C-Mod develops a reproducible ITB with a very steep electron density profile (see Figs. 1-2). Ion and electron thermal confinement are found from experimental analysis to be better than neoclassically predicted in the plasma core. A typical such experiment is analysed here, pulse #1001220016. It is characterized by R_o= 0.69 m, B_o= 4.5 T, Ip=0.78 MA, central electron density = $4\text{x}10^{20}/\text{m}^3$. Deuterium majority ion and impurities of oxygen, carbon, boron and molybdenum give $<Z_{eff}>\sim 1.64$. Plasma central beta is less than 1%. Toroidal rotation is found to reverse sign as the barrier is established.

The ITB exhibits steep, spontaneous density peaking, a reduction in particle transport occurring without a central particle source. The ITB development occurs in the early phase of a dual frequency RF experiment, which shows density control with central RF heating later in the discharge. In Fig. 2 are time slices of the radial profiles of the plasma electron density, electron temperature and ion temperature. We consider only the "trigger time", 0.9 sec, just before the ITB is established, to identify the plasma conditions conducive to ITB formation. For this ICRF EDA H-Mode, the minority resonance is at $r/a\sim 0.5$ on the high field side, beginning at 0.7 sec. EDA refers to edge D_α radiation, which is high for high performance H-modes at high densities and temperatures. Since the central temperature is maintained while the central density is

increasing, this also suggests that a thermal transport barrier exists[11], in addition to the barrier to particle transport evident in Fig. 2a. Sawtooth heat pulse propagation experiments[12] show that the ITB is limited to a very localized region (Fig 3.).

The experiment has been analysed with the TRANSP code[17], including a sawtooth model which causes the safety factor, q, to drop below unity by ~ 10% at each sawtooth. The TRANSP results were processed with GS2_PREP[18] for GS2 input, averaging over 50 ms at the time of interest. As the sawtooth period is 10 ms, a sawtooth-averaged condition is used for the simulations. The key input variables for each radius simulated are found in Table I. The plasma had a normal shear profile, with q monotonic. Error in the experimental measurements of all data is estimated to be on the order of 10-20%. The impurity and minority ions at the "trigger" time are estimated to be 3% boron and 4% hydrogen. The walls of C-Mod are molybdenum, regularly coated with boron (from D_2B_6 boronization) for edge density control. Examination of bolometer profiles indicates molybdenum levels < 0.1%. The low Z impurity level is estimated at 3% from visible bremsstrahlung measurements, yielding Z_{eff}. The impurity ion is identified as boron, although the low Z impurities may be actually 2% boron and 1% carbon. Boron and carbon are so similar in collisional properties that only boron impurity ions are included in the simulations. No oxygen is thought to have been present. The hydrogen to deuterium ratio, 4% at the trigger time, was obtained from spectroscopic measurements of D_α and H_α radiation.

Radio frequency heating of the hydrogen minority causes the hydrogen temperature ($T_h=2E_h/3k$) to be peaked around the half radius[19], with a less radially peaked hydrogen density profile. The ion distribution function is not thought to have a high energy RF tail, due to the high density and collisionality. $\boldsymbol{E\times B}$ shearing rates can be estimated from measurements of toroidal

rotation but at the time of interest, the toroidal rotation is near zero, changing from co to counter rotation as the ITB is established.

Electron temperature data for the TRANSP analysis was taken from Thomson scattering as the electron cyclotron emission (ECE) signal is cut off during the ITB because of rising high electron density. The density profile data was obtained from inverted visible bremstrahlung measurements, adjusted for the Z_{eff} and temperature dependence. The plasma ion temperature profile in TRANSP was calculated on the basis of neutron data and the assumption that χ_i is proportional to the neoclassical ion diffusivity[20], $\chi_i^{Chang\text{-}Hinton}$. This leads to $T_i(r)$ being broader, and slightly lower than $T_e(r)$. While the high density of C-Mod suggests that $T_i = T_e$ would be a good assumption in the plasma core, the data are consistent with either ion thermal loss model.

III. GS2 MICROSTABILITY CODE

The transport of particles and energy in high temperature fusion plasmas is widely believed to result from the turbulence of drift wave fluctuations. Presently however, a complete, theory-based calculation of such microturbulence throughout the experimental plasma volume is not feasible. In this paper, drift wave microturbulence stability simulations along single flux-tubes are reported, to test the concept for a specific experiment.

The calculations were primarily carried out with the GS2 gyrokinetic microinstability code[6,7], which is based on the electromagnetic nonlinear gyrokinetic equation[21-25]. This equation describes the evolution of small turbulent fluctuations in particle and field quantities which satisfy

$$\frac{\tilde{h}}{F_0} \sim \frac{e\tilde{\phi}}{T} \sim \frac{\tilde{A}_{//}}{B\rho} \sim \frac{\tilde{B}_{//}}{B} \sim \frac{\rho}{\lambda} \sim \frac{\rho}{L} = \delta << 1, \qquad k_{//}L \sim k_{\perp}\rho \sim 1. \tag{1}$$

Here $\tilde{h}$ is the nonadiabatic part of the perturbed distribution function, F_0 is the equilibrium distribution function, $\tilde{\phi}$ and $\tilde{A}_{//}$ are the perturbed parts of the electrostatic and parallel vector

potential, $\tilde{B}_{//}$ is the perturbed parallel magnetic field, B is the equilibrium magnetic field, L is an equilibrium scale length (of density, temperature, or magnetic field), and $\square=eB/(mc)$ and $\square=v_t/\square$ are the cyclotron frequency and thermal gyroradius of a given particle species with thermal velocity $v_t^2 = T/m$ and charge e. The simulations are performed in field-line-following coordinates using toroidal flux tubes[26-28]. In such coordinates, the nonlinear gyrokinetic equation may be written as

$$(\frac{d}{dt} + \mathrm{v}_{//}\mathbf{b}\cdot\square + i\square_d)\tilde{h} = i\square_{\square}^T\square\square e\frac{\partial F_0}{\partial\square}\frac{\partial\square}{\partial t}. \tag{2}$$

Here the distribution function $F_0=F_0(\square\square)$ depends only on the energy $\square=mv^2/2$ and the flux surface label $\square$, where $\square$ is the equilibrium poloidal magnetic flux enclosed by the magnetic surface of interest. The total time derivative is given by $d_t=\partial_t+(c/B)[\square,\cdot]$, where $[\cdot,\cdot]$ is the Poisson bracket. The perpendicular curvature and $\square B$ drifts are given by

$$\square_d = \boldsymbol{k}_{\square}\cdot\boldsymbol{B}\square(m\mathrm{v}_{//}^2\boldsymbol{b}\cdot\square\boldsymbol{b} + \square\square B)/(Bm\square), \tag{3}$$

where $\square= \mathrm{mv}_{\square}^2/(2\mathrm{B})$ and the fields are represented by

$$\square = J_0(\square)(\tilde{\square}\square\frac{\mathrm{v}_{//}}{c}\tilde{A}_{//}) + \frac{J_1(\square)}{\square}\frac{m\mathrm{v}_{\square}^2}{e}\frac{\tilde{B}_{//}}{B}. \tag{4}$$

Here, $\square = k_{\square}\, v_{\square}/\square$ and $\square_{\square}^T = n_0 c\partial_{\square}F_0$, where n_0 is the toroidal mode number of the perturbation. The self-consistent electromagnetic field fluctuations are computed from the gyrokinetic Poisson-Ampere equations,

$$\square_{\square}^2\tilde{\square} = 4\square\square_s e\square d^3r[e\tilde{\square}\frac{\partial F_0}{\partial\square} + J_0(\square)\tilde{h}], \tag{5}$$

$$\square_{\square}^2\tilde{A}_{//} = \square\frac{4\square}{c}\square_s\square d^3r[e\mathrm{v}_{//}J_0(\square)\tilde{h}], \tag{6}$$

$$\frac{\tilde{B}_{//}}{B} = \square\frac{4\square}{B^2}\square_s\square d^3r[m\mathrm{v}_{\square}^2\frac{J_1(\square)}{\square}\tilde{h}]. \tag{7}$$

The Bessel functions J_0 and J_1 arise because equations 5-7 are formulated in particle space **x**, rather than in gyrocenter space **R**. We retain the Debye-shielding term $\lambda_{De}^2 \tilde{\phi}$ in Poisson's equation, since the electron Debye length λ_{De} can be comparable to ρ_e in laboratory fusion experiments. Of course this term can be neglected when only ion-scale instabilities are studied.

GS2 is a nonlinear generalization of a widely used gyrokinetic stability code[6]. An operator splitting scheme is use, so that the linear terms, including equations 5-7, may be treated implicitly. The nonlinear terms are evaluated with a dealiased pseudospectral algorithm in the plane perpendicular to the field line. A second-order Adams-Bashforth scheme is used to advance the nonlinear terms in time. Non-uniform coordinate meshes are used in velocity space to improve the resolution, particularly for the trapped-passing boundary. A small amount of upwind diffusion is typically used, only in the direction along the field line. In the absence of upwind diffusion, the algorithm is second-order accurate in space and time. Good parallel performance is achieved by employing multiple-domain decomposition in four of the five dimensions at all times.

This initial value code solves for the perturbed eigenfunctions of the electrostatic potential ϕ and the components of the electromagnetic potential, $\boldsymbol{A}$, parallel and perpendicular to the field line direction. The ballooning representation along a field line is chosen for model simplicity with, for example, the perturbed electrostatic potential eigenfunction written

$$\tilde{\phi}(r,\theta,\zeta,t) = \exp[in\zeta - inq(r)\theta] \sum_{p=-\infty}^{p=\infty} \tilde{\phi}(\theta - 2\pi p, r, t) \exp[inq(r)2\pi p] \qquad (8)$$

Here (r,θ,ζ) are the usual radial, poloidal angle and toroidal angle coordinates. To illustrate the highly nonlinear nature of the drift wave microstability calculation, the linearized gyrokinetic equation, using the "s-α" MHD equilibrium is written:

$$\frac{\partial}{\partial t}\tilde{g}_s + \frac{v_{//}}{qR}\frac{\partial}{\partial\theta}\tilde{g}_s + i\omega_{ds}\tilde{g}_s + C(\tilde{g}_s) = \frac{e_s}{T_s}F_{ms}\left(\frac{\partial}{\partial t} + i\omega^T_{*s}\right)\left\{\left[\tilde{\phi}(\theta) - \frac{v_{//}}{c}\tilde{A}_{//}(\theta)\right]J_0 + \frac{J_1(\lambda)}{\lambda}\frac{mv_\perp^2}{e}\frac{\tilde{B}_{//}}{B}\right\} \quad (9)$$

where

$$\tilde{g}_s \equiv \tilde{f}_s + \left(\frac{e_s}{T_s}\right)F_{ms}\tilde{\phi}(\theta),$$
$$\omega_{ds} = \omega_{*s}(L_{ns}/R)(E/T_s)(1 + v_{//}^2/v^2)\{\cos\theta + [\tilde{s}\theta - \alpha\sin\theta]\sin\theta\}$$
$$k_\theta = -nq/r$$
$$k_\perp = k_\theta\{1 + [\tilde{s}\theta - \alpha\sin\theta]^2\}^{1/2}$$
$$\tilde{s} \equiv (r/q)(dq/dr)$$
$$\alpha \equiv -q^2R(d\beta/dr)$$
$$\omega^T_{*s} \equiv \omega_{*s}\{[1 + \eta_s[E/T_s) - 3/2]\}$$
$$J_0 \equiv J_0(k_\perp v_\perp/\Omega_s)$$
$$\omega_{*s} \equiv kT_s(-n_s/n_s)/e_sB$$
$$L_{ns} \equiv -(n_s/-n_s)$$
$$\eta_s \equiv d\ell nT_s/d\ell nn_s$$

(Note however that a numerically calculated MHD equilibrium is used in the rest of this paper, not the s-α model equilibrium.)

In general, driving forces for the microturbulence arise from temperature and density gradients in ω_{*s}, mediated by the effects of passing ions and of trapped electrons. Stabilization of turbulence is achieved through high values of shear, q, α, impurities, collisional effects, and nonzero T_e. The competition among many driving and stabilizing forces requires computational methods to analyse a particular experimental situation.

IV. GYROKINETIC SIMULATION RESULTS

We examine only the time just before the ITB is established, and the plasma density peaking begins. Three zones characteristic of the experimental conditions are simulated: the plasma core at ~0.25*r/a*, the region where the ITB occurs at ~0.45*r/a* and outside the ITB at ~0.65*r/a*. The calculations were carried out at the USDOE NERSC Cray T3E and IBM RS/6000SP computers using a total of ~50,000 hours, with runs typically making use of 40-256 parallel processors.

A. Linear simulations

The linear simulations are fully electromagnetic, include the nonadiabatic electron response, and four plasma species: electrons, deuterium, boron impurity and fast hydrogen ions. They cover the full range of drift mode wavevectors, including ion temperature gradient mode (ITG), trapped electron mode (TEM) and electron temperature gradient mode (ETG) wavelengths, $k_\theta \rho_i$ = 0.1 to 80 (Figs. 4, 5). We will denote by ITG-TEM microturbulence from $k_\theta \rho_i$ = 0.1 to 1, as these instabilities are hybrid modes characterized by both ITG and TEM behavior. From $k_\theta \rho_i$ = 2 to 10 the instabilities are TEM, while above $k_\theta \rho_i$ = 10 the microturbulence is pure ETG, driven by passing electrons only. The simulations solve the gyrokinetic Vlasov-Maxwell system and are run out for 10,000 time steps, until the microinstability growth rates, γ, and real frequencies, ω, are verified to have converged and the usual measure of the electrostatic potential, $ln|\phi|^2$, is verified to be linearly increasing, in cases that are designated unstable.

The stability analysis shows that in the barrier region (*r/a* ~ 0.45) no ITG-TEM mode is strongly growing for $0.2 < k_\theta \rho_i < 0.8$, while outside the ITB region a clear ITG-TEM signature is found. In the plasma core there are no strongly growing modes at $0.5 \leq k_\theta \rho_i \leq 0.8$ and only poorly resolved modes with $\omega < 0$, electron diamagnetic direction) are unstable at $k_\theta \rho_i \leq 0.4$. The

apparently unstable mode at $k_\theta \rho_i$ = 0.1 is not converged and does not have a well defined eigenfunction. At higher values of $k_\theta \rho_i$, the TEM (usually found near $k_\theta \rho_i$ ~ 1) is stable everywhere. The ETG (peaked at $k_\theta \rho_i$ ~ 25) is strongly unstable outside and at the barrier, but is stable in the core.

Anomalous χ_i is associated with ITG-TEM instability, so that we expect reduced ion thermal confinement at, and within the ITB. TRANSP shows that χ_{eff} drops inside the ITB[11]. Anomalous χ_e is associated with strong ETG, and the mixing length model would predict 1/2 for the ratio of χ_e at the ITB to that outside. Sawtooth heat pulse propagation measurements of similar experiments have shown that the effective $\chi^{heatpulse}$ is reduced (by factor ~ 10) in a narrow radial region of ~ 1 cm, located near the foot of the particle barrier, but not necessarily within the barrier[12]. Reduced microinstability growth rates predicted at the barrier are consistent with this observed reduced transport. The nonlinear calculations, however, report such an order of magnitude decrease in χ_e in the next section.

The sensitivity of the microturbulent stability in the ITB region has been examined through the response of the calculated real frequencies and growth rates to variation of specific driving forces across the plasma. Figure 6 shows the radial variation of the dimensionless drift mode driving and stabilizing parameters for the experiment at the trigger time. We find that χ_i increases as *r/a* increases, as does the normalized electron temperature gradient. These and the decreasing normalized impurity gradient for the primary impurity, boron (3%), are consistent with stabilized ITG-TEM in the core. Removal of the boron impurity, while maintaining charge neutrality with Z_{eff} =1 destabilizes the ITG-TEM in the barrier region. Similarly removal of the 4% hydrogen species while maintaining ambipolarity also destabilizes the ITG-TEM mode in the barrier region.

It is found in this case, that either decreasing the plasma electron density gradient or increasing the plasma electron temperature gradient causes the ITG-TEM mode to be destabilized in the transport barrier region. Near marginal stability where gyrokinetic calculations, rather than fluid calculations are needed, the instability is expected to grow linearly according to $\gamma = A\nabla T/T + Bn/\nabla n$, where A and B depend on specific plasma conditions. Far from marginal stability the fluid approximation is useful; the instability is strong, becoming pressure gradient driven so that temperature and density gradients add up with equal weight $(1+\tau_i)$. Near marginal stability, as in this case the ITG-TEM is ion temperature gradient driven. The behavior of the ITG-TEM mode is complex and controlled by nonlinear equations, as seen in Sec. III. Romanelli's kinetic theory treatment has shown that density peaking may stabilize or destabilize the ITG-TEM mode, depending on plasma collisionality, trapped electron fractions and T_i/T_e[29].

For the C-Mod ITB trigger time, we find the growth rates in the barrier region are more strongly elevated (factor 25) by doubling $-\nabla T/T$ than by reducing $-\nabla n/n$ by two. Critical temperature gradients have been examined (Fig. 7) and show that the barrier region is far above destabilization through reduced density gradients, but is very close to marginal stability considering only increased temperature gradients. The measured normalized temperature and density gradients are 2.0 and 0.6 (Table I).

B. Nonlinear simulations

Nonlinear electrostatic simulations were carried out for the three zones, under the same initial conditions. These simulations followed four plasma species, as did the linear simulations, but represent the interaction of a limited group of modes, keeping four values of k_θ and 23 values of k_r. For this low beta experiment, there should be no difference in results compared to the

corresponding nonlinear electromagnetic calculations, and electrostatic calculations are more efficient, requiring one-third the computational cost.

Just as the linear calculations showed stable long wavelength turbulence at the ITB region, without invoking suppression by $\boldsymbol{E}\times\boldsymbol{B}$ shear at the trigger time, the nonlinear simulations of the C-Mod plasma also show quiescent microturbulence in the ITG-TEM range of frequencies in the barrier region, just before ITB formation (Fig. 8).

In Figs. 9-11 are shown the simulation results for the nonlinear evolution of the plasma quasineutrality, $(n_e-n_d-5n_b-n_h)/n_e$, and for the particle and heat fluxes of the electron, deuterium and boron ion species. Maintaining quasineutrality is an important check of simulation validity. We find that the quasineutrality in the plasma core is maintained to less than 1%, to much less than 1% in the barrier region, and to about 1% outside the barrier. In the plasma core, the particle flux is outward, with the electron and deuterium fluxes being of similar magnitude, and the heat flux is also outward, with the electron heat flux being greater than the deuterium heat flux. In the barrier region, before ITB formation, the particle flux from electrons and deuterium is inward, with electron and deuterium fluxes of similar magnitude, while the heat flux is outward, with the deuterium heat flux being greater (~3x) than the electron heat flux. Outside the ITB region, the particle flux is inward, with electron flux ~30% greater than the deuterium flux; the heat flux is outward, with the deuterium heat flux being much larger (~5x) than the electron heat flux. The boron carries negligible particle and heat flux. Bursting behavior is evident in the fluctuating microturbulence. Similar results have been found in a separate study of this discharge[30], which primarily examines the role of the TEM instability and which shows stability for ITG before the trigger time in the barrier region.

C. Comparison with experiment

In the plasma core, GS2 predicted weak turbulence, with saturation occurring along with the development of a 77 kHz Geodesic Acoustic Mode (GAM) (see Fig. 8). A high frequency core mode at 80 kHz for a similar C-Mod experiment has been found with ECE[31]. The simulated mode is a stable mode of the plasma, excited as a damped computational mode. The GAM depends only on the device size and the plasma temperature. In the experiment such a stable mode may have been driven unstable by RF heating. The only well resolved linearly unstable mode in this frequency range in the simulations is an ITG-TEM mode at about 50 kHz, outside the ITB region.

Particle and heat fluxes from the gyrokinetic calculations and from the TRANSP experimental analysis are shown in Table II. Although this is not a steady state experimental condition, the correlation time of the simulated fluctuations will be of the order of microseconds, much shorter than the time scale of the evolving plasma (msec), and it is worthwhile to compare the simulation fluxes to experiment.

The experimental fluxes are obtained from the TRANSP analysis at the time of interest, for radial zones of width $1/20^{th}$ of the minor radius. Because the H-mode density gradient is low at this time, error bars for particle fluxes and diffusivities are quite large. The TRANSP analysis results were averaged at 0.9 sec over ±50 ms., just as was done to determine the input parameters for the GS2 simulations.

As can be seen from Figs. 9-11, the error bars on the GS2 results are as large as the fluxes and transport coefficients themselves. The GS2 results have been averaged over the full simulation times, after the linear growth and initial saturation phases. While the GS2 electrostatic potential evolution, as shown in Fig. 8, has reached reasonable steady state values, with moderate

fluctuation levels, the heat and particle fluxes of Figs. 9-11 show considerable intermittency with indication of decreasing trends in the average fluxes. The difference in moments of k in each affects their different time dependent trends.

In the plasma core χ_e and χ_i agree within a factor of two with experimental analysis. No ***ExB*** correction has been applied or appears needed, as the toroidal velocity is measured to be very small at the plasma center at the trigger time.

The quiescent turbulence calculations of plasma flux in the ITB region are small, but may be of quantitative significance when compared with the sawtooth heat pulse experimental χ_{eff} which is very small near the barrier region (Fig. 3). TRANSP (Table II) does not have the resolution of such diagnostics, The flux tube calculations may properly represent very low plasma heat transport there.

The microturbulence simulations within and outside the barrier region, however, overestimate the average values of the particle and heat fluxes compared to the experimental analysis code. Clearly better statistics are needed for useful comparisons of microturbulent plasma simulations with experimental data analysis. Future work should extend the simulations at least five to ten times longer than shown here.

If we compare our results to those for other tokamak experiments, both gyrofluid[15] and recent gyrokinetic simulations[30,32-34], we find that ***ExB*** corrections are critical for satisfactory comparison with experiment. For the DIII-D L-mode, gyrofluid calculations[15] including shear flow corrections, underestimated particle fluxes by less than a factor of five, and agreed with heat flux data within a factor of two for both ions and electrons. Nonlinear gyrokinetic simulations[32] of the energy fluxes for the same discharge are comparable but higher than the gyrofluid simulations. When corrected for ***ExB*** flow shear, they exceed the experimental ion

thermal transport by more than a factor of 2, and overestimate the density fluctuation level. Nonlinear gyrokinetic simulations of the Alcator C-Mod ITB H-mode during on-axis heating[30] are also in agreement with measurements of particle and heat fluxes within experimental error bars. Nonlinear, global gyrokinetic simulations[33] of DIII-D L-mode discharges have matched the measured energy diffusivities within experimental uncertainty, about a factor of two for ions and about 20% for electrons. But in simulations[34] of highly anomalous experiments on DIII-D with extreme reversed shear, and on JET including a current hole, gyrokinetic calculations, not corrected for shear flow, found that the simulated and measured plasma fluxes differed by factors as high as 40 to 10^3.

The large differences in simulated and experimental average values for the ion heat flux and diffusivity in the region outside the ITB suggests that physics may be missing from the simulations. The toroidal velocity appears to be near zero in the single point measurement near the plasma center, but since the velocity is changing throughout the experimental pulse there may be shear flow outside the ITB, which if included in the calculation would suppress ITG turbulence. In addition if the ITG turbulence is near the critical gradient, small changes in the ion temperature gradient can cause large changes in the simulated turbulent fluxes. One or both of these effects could be responsible for the overestimates of average ion heat and particle fluxes from the simulated ITG turbulence outside the barrier region. Clearly the best possible experimental data is needed for reliable comparison with simulations. It is hoped that future experiments will include improved plasma rotation and ion temperature measurements. We note that good confinement is found in these simulations to result from high values of $\nabla n/n$ and low $\nabla T/T$ in the ITB region, which stabilize the turbulent microstabilities near the plasma core.

D. Discussion

The gyrokinetic model calculations show that just before ITB formation, conditions have already been established for which a peaked density profile will occur and be sustained. Good confinement is found in these simulations to result from high values of $-\nabla n/n$ and low $-\nabla T/T$ in the ITB region, which stabilize the turbulent microstabilities near the plasma core. The Ware pinch provides sufficient fueling to account for a sustained ITB peaked density profile[19]. Since we find no strong drift wave instabilities at the ITB region, microturbulent driving forces are not strong enough to provide the usual anomalous transport across the barrier region. Outside the core plasma, ITG-TEM and ETG drift modes are linearly unstable.

Identification of the driving forces responsible for drift wave microstability in the barrier region before the ITB appears, was explored by examining the effects of changing the gradients of the magnetic shear, the densities and temperatures of the electron and ion species. It was found that increase in the normalized electron temperature gradient, $-\nabla T/T$, caused the largest destabilization of the ITG-TEM mode in the barrier region at the trigger time. Linear sensitivity studies show that increasing the normalized temperature gradients, and reducing normalized density gradients, $-\nabla n/n$, as well as increasing the plasma safety factor at the ITB location, would destabilize the ITG-TEM mode frequencies and would likely prevent ITB formation.

This suggests that the ITB is triggered by reduction in the normalized electron temperature gradient driving force for the ITG-TEM and ETG microstability when off-axis RF heats the plasma locally. This would explain the observation of ITB with off-axis but not on-axis RF, as due to weaker $-(\nabla T_e)/T_e$ at the barrier region. The C-Mod ITB studied here formed spontaneously, during an off-axis RF-heated H-mode. This occurs during the EDA H-mode, characterized by edge D_α radiation, but not during the elm-free H-mode, which occurs at lower

plasma density. Microstability analysis for the elm-free H-mode, which does not lead to an ITB with similar off-axis RF heating, as well as for the trigger time of the spontaneously occurring ohmic H-mode ITB[11] will be important to contrast to this case, to clarify the ITB formation process. Weaker $-(\nabla T_e)/T_e$ at the barrier region does not occur at the trigger time in the ohmic H-mode. Because there are so many plasma forces, which can nonlinearly affect drift wave microstability, it would not be surprising to find that different processes are responsible for ITB formation in different experimental scenarios.

V. CONCLUSION

The ITB during off-axis RF heating on C-Mod has been examined with gyrokinetic calculations in flux tube geometry. Linear and nonlinear calculations, including electrostatic and fully electromagnetic treatments, with the complete electron response, and following four plasma species, show ITG-TEM microturbulence is already suppressed in the ITB region before formation, at the trigger time, without recourse to the usual requirements of velocity or magnetic shear[3]. The microstability analysis is qualitatively consistent with the experimental transport analyses, showing high transport outside and inside the ITB region before formation. Strong ITG-TEM and ETG drift wave turbulence are identified outside the barrier region, with reduced ETG (short wavelength) turbulence found in the ITB region. Nonlinear calculations support the linear stability results and demonstrate the saturation of core, ITB and outer plasma microturbulence.

The microstability analysis shows that, in this case, linear, flux tube calculations are sufficient for understanding the microscopic basis of drift mode ITG turbulence suppression on C-Mod. While the heuristic picture provided by linear calculations is supported by the nonlinear results, detailed agreement of particle and heat fluxes are only in agreement with measurements

within large experimental and simulation error bars. Better diagnostics are desirable since drift wave instabilities are extremely sensitive to the plasma profiles and to magnetic and velocity shear. It is interesting that recent flux-tube, fully electromagnetic gyrokinetic simulations of microturbulence on the National Spherical Tokamak Experiment (NSTX)[35] do not reflect so clearly the connection between drift mode instability and observed transport[36]. The tokamak paradigms for drift mode microturbulence and transport coefficients may need modification in application to the spherical torus and the geometries of other fusion devices.

The conditions for formation of this type of ITB on C-Mod, diagnosed with gyrokinetic calculations, suggest that ***ExB*** shear is not required. Future work may identify experimentally verifiable trigger mechanisms. In this case, reduced $-(\nabla T_e)/T_e$ appears to be the primary stabilizing force on the ITG-TEM mode, although many other plasma parameters have been shown to be destabilizing. In other types of ITB experiments, one or more other plasma conditions may be controlling barrier formation. Establishment of ITB without the requirement of ***ExB*** shear, as for this experiment, may yield practical and economic benefits for fusion reactor operation.

ACKNOWLEDGEMENT

We are glad to acknowledge the experimental and diagnostic teams at Alcator C-Mod, which provided the data and basis for the analysis in this paper. We especially wish to acknowledge discussions with S. Wolfe, B. Lipschultz, J. Terry and M. Greenwald at MIT. Valuable and interesting conversations with G. Hammett, E. Belli, R. Budny, and W. Lee of Princeton Plasma Physics Laboratory, Princeton University, and C. Bourdelle, Euratom-CEA, France, were key to completing this study. We also thank G. Schilling, PPPL, and E. Marmar and M. Porkolab, MIT, for their support. Research was carried out under U. S. DOE Contract DE-AC02-76CH03073.

References

[1] W. M. Tang, Phys. Plas**. 9** (2002) 1856.

[2] W. Horton, Rev. Mod. Phys. **71** (1999) 735-776.

[3] P. W. Terry, Rev. Mod. Phys. **72** (2000) 109-165.

[4] K. Itoh, Nucl. Fusion **43** (2003) 1710-1719.

[5] I. H. Hutchinson, R. L. Boivin, F. Bombarda *et al*., Phys. Plas. **1**, 1511 (1994).

[6] M. Kotschenreuther, G. Rewoldt and W. M. Tang, Comp. Phys. Comm. **88**, 128 (1995).

[7] W. Dorland, F. Jenko, M. Kotschenreuther and B. N. Rogers, Phys. Rev. Lett. **85**, 5579 (2000).

[8] "ITER Physics Basis", Nuclear Fusion, **39** (1999) 2137-2638.

[9] M. H. Redi*,* C. Fiore, P. Bonoli*, et al*., Proceedings of the 29th EPS Conference on Plasma Physics and Controlled Fusion, Montreux, Switzerland, 2002, edited by R. Behm, C. Varandas (European Physical Society, Lausanne, 2002) Vol. 26B, Paper 1.082.

[10] M. H. Redi, R. Bell, P. Bonoli *et al*., Proceedings of the 30th EPS Conference on Plasma Physics and Controlled Fusion, St. Petersburg, Russia, 2002, edited by R. Koch, S. Lebedev (European Physical Society, Lausanne, 2002), Vol. 27A, Paper P4.94.

[11] C. L. Fiore, J. E. Rice, P. T. Bonoli, *et al*., Phys. Plas. **8,** 2023 (2001).

[12] S. Wukitch, R. L. Boivin, P. T. Bonoli, *et al.,* Phys. Plas. **9**, 2149 (2002).

[13] J. E. Rice, P. T. Bonoli, E. Marmar, *et al.,* Nuclear Fusion **42** (2002) 510.

[14] R. E. Waltz, G. D. Kerbel, J. Milovich, G. W. Hammett Phys. Plas. **2** 2408 (1995).

[15] D. W. Ross, R. V. Bravenec, W. Dorland, *et al.* Phys. Plas. **9** (2002) 177-184.

[16] R. V. Budny, R. Andre, A. Becoulet, *et al*. Plasma Physics and Controlled Fusion **44** (2002) 1275-1228.

[17] R. J. Hawryluk, in *Physics of Plasmas Close to Thermonuclear Conditions*, edited by B. Coppi, G. G. Leotta, D. Pfirsch, R. Pozzoli, and E. Sindoni (Pergamon, Oxford, 1980), Vol. 1, p. 19.

[18] D. Ernst, R. E. Bell, M. G. Bell, *et al.* Phys. Plas. **7** (2000) 615-625.

[19] P. Bonoli, *et al,* 18th IAEA, Sorrento, Italy, IAEA-CN-77, EXP4/01 (Oct.,2000.)

[20] C. S. Chang, F. L. Hinton, Phys. Fluids **25**, 1493 (1982).

[21] T. M. Antonsen and B. Lane, Phys. Fluids **23**, 1205 (1980).

[22] E. A. Frieman and L. Chen, Phys. Fluids **25**, 502 (1982).

[23] R. G. Littlejohn, J. Plasma Phys. **29**, 111 (1983).

[24] T. S. Hahm, W. W. Lee and A. Brizard, Phys. Fluids **31**, 1940 (1988).

[25] A. Brizard, J. Plasma Phys. **41**, 541 (1989).

[26] S. C. Cowley, R. M. Kulsrud and R. Sudan, Phys. Fluids **B3**, 2767 (1991).

[27] K. V. Roberts and J. B. Taylor, Phys. Fluids **8**, 315 (1965).

[28] M. A. Beer, S. C. Cowley and G. W. Hammett, Phys. Plasmas **2**, 2687 (1995).

[29] F. Romanelli and S. Briguglio, Phys. Fluids **B2** (1990) 754.

[30] D. R. Ernst, P. T. Bonoli, P. J. Catto*, et al*., "Role of trapped electron mode turbulence in internal barrier control in Alcator C-Mod", Phys. Plas. in press (2004).

[31] A. Lynn, P. E. Philips, M. B. Sampsell, *et al.,* 45th Annual Meeting of the Division of Plasma Physics (2003) Albuquerque, NM, Bull. Am. Phys. Soc. FP1.009, "Heterodyne ECE Observations of Coherent Modes in Alcator C-Mod"

[32] D. W. Ross, W. Dorland, Phys. Plas. 9 (2002) 5031-5035,

[33] R. V. Budny, R. Andre, C. D. Challis, *et al.* Proceedings of the 30th EPS Conference on Plasma Physics and Controlled Fusion, St. Petersburg, Russia, 2002, edited by R. Koch, S. Lebedev (European Physical Society, Lausanne, 2002), Vol. 27A, Paper O-3.4A(P3.88).

[34] J. Candy and R. E. Waltz, Phys. Rev. Lett. 91 (2003) 045001-1.

[35] M. Ono, S. M. Kaye, Y.-K. M. Peng *et al*. Nucl. Fusion, **40**, 557 (2000).

[36] M. H. Redi, W. Dorland, J. Candy*, et al.,* 45th Annual Meeting of the Division of Plasma Physics (2003) Albuquerque, NM, Bull. Am. Phys. Soc. KO1.007, ”Gyrokinetic Calculations of Microturbulence and Transport in C-Mod and NSTX”.

Table I. Plasma parameters for simulation of three zones at the trigger time for ITB formation in the off-axis RF heated H-mode on C-Mod. The ratios of deuterium to electron density is 0.8, of boron to electron density is 0.03, and of hydrogen to electron density is 0.04 at all radii.

Parameter	r/a~0.25	0.45	0.65
q	0.998	1.3	2.00
$\hat{s}$	0.12	0.87	1.52
T_e/T_d	1.04	0.87	0.95
T_d/T_d	1.00	0.99	1.01
T_b/T_d	1.00	0.99	1.01
T_h/T_d	1.32	4.57	1.57
$-a_{ref}\nabla n_e/n_e$	0.57	0.60	0.06
$-a_{ref}\nabla n_d/n_d$	0.57	0.60	0.06
$-a_{ref}\nabla n_b/n_b$	0.57	0.60	0.06
$-a_{ref}\nabla n_h/n_h$	0.58	0.60	0.05
$-a_{ref}\nabla T_e/T_e$	1.18	2.00	2.76
$-a_{ref}\nabla T_d/T_d$	0.49	1.75	3.24
$-a_{ref}\nabla T_b/T_b$	0.50	1.75	3.25
$-a_{ref}\nabla T_h/T_e$	0	0	0
Δ_e	0.28	0.46	1.21
Δ_d	0.24	0.24	0.24
Δ_b	0.25	0.25	0.25
Δ_h	0	0	0

T_{ref}(keV)	1.16	0.97	0.54
a_{ref} (m)	0.22	0.22	0.22
$n_{ref} = n_e$ (m^{-3})	3.2×10^{20}	2.8×10^{20}	$2.7 e \times 10^{20}$
$\square_{ref}$	0.007	0.005	0.003
Freq norm=$(T_{ref}/m_{ref})^{0.5}/a_{ref}$ (sec^{-1})	1.1×10^{6}	9.8×10^{5}	7.3×10^{5}
$\square_{ref}$ norm = $k_{\square}^{-1}$ (cm)	0.120	0.119	0.094

Table II. Particle fluxes, heat fluxes and transport coefficients at three flux surfaces of the pre-ITB plasma from GS2 gyrokinetic calculations and TRANSP physics analysis. Ion fluxes are combined results for deuterium and boron. The zones are at r/a~ 0.25, 0.45 and 0.65. $\chi_i^{neoclassical}$ is ~ 0.3m^2/sec

	S_i (10^{20}/m^2-sec)	S_e (10^{20}/m^2-sec)	Q_i (MW/m^2)	Q_e (MW/m^2)	D (m^2/sec)	χ_i (m^2/sec)	χ_e (m^2/sec)
GS2							
core	2.3(±2.3)	2.5(±2.5)	0.09(±0.09)	0.17(±0.17)	0.31(±0.31)	0.63(±0.63)	0.54(±0.54)
ITB	-0.9(±0.9)	-0.9(±0.9)	0.03(±0.03)	0.01(±0.01)	-0.12(±0.12)	0.09(±0.09)	0.03(±0.03)
Outside	-116(±116)	-149(±149)	17(±17)	3.2(±3.2)	-203(±203)	49(±49)	11(±11)
TRANSP							
core	-0.1(±0.3)	-0.2(±0.4)	0.04(±0.04)	0.1(±0.04)	-0.02(±0.05)	0.4(±0.3)	0.3(±0.1)
ITB	-0.2(±0.5)	-0.3(±0.6)	0.1(±0.1)	0.4(±0.1)	-0.1(±0.1)	0.4(±0.2)	1.4(±0.3)
outside	-0.1(±0.7)	-0.3(±0.9)	0.1(±0.1)	0.5(±0.1)	-2.(±2.)	0.4(±0.3)	2.2(±0.6)

Figure Captions

Fig 1: C-Mod ITB discharge with off-axis ICRF heating throughout the discharge and central ICRF heating applied after ITB established. Summary traces are ICRF power, stored plasma energy, average density, neutron rate, ion temperature and toroidal rotation. Figure reproduced from Ref. 12, used with permission of the author.

Fig 2: a) Electron density (10^{14}/cm^3) versus radius (*r/a*) showing evolution from ohmic and L-mode phases to RF H-mode and the ITB, density peaked phase. Timeslices show density becoming more peaked every 0.2 sec, from 0.5 to 1.2 sec, and then the central density showing a small decrease at 1.4 sec. The time of interest is 0.9 sec, before the ITB is established. The three radial locations for the gyrokinetic calculations are shown at *r/a*~0.25, 0.45 and 0.65.

b) Electron temperature profile time slices, as in Fig. 2a for electron density. Similar dotted/dashed patterns are used as for Fig. 2a. The profile for 0.9 sec is indicated.

c) Ion temperature profile time slices, as in Fig. 2a for electron density. Similar dotted/dashed patterns are used as for Fig. 2a. The profile for 0.9 sec is indicated.

Figure 3. Comparison of the experimental (squares) and simulation (dimonds) time-to-peak data show good agreement for the assumed χ^{hp} profile (solid line). This indicates that the region of improved confinement is restricted to a narrow radial layer. Outside this region there is little evidence of improved transport. Figure reproduced from Ref. 12 , used with permission of the author.

Figure 4. Real frequencies (~10^6/sec) of drift mode microturbulence from linear calculations for $k_\theta \rho_i$ from 0.1 to 80. Calculations were fully electromagnetic, included four species and the complete nonadiabatic electron response for radial zones inside, at and outside the ITB region.

Figure 5. a) Growth rates (~10^6/sec) from linear calculations for $k_\theta \rho_i$ from 0.1 to 80, the ITG-TEM, TEM and ETG range of wave vectors. ITG-TEM is unstable outside the core, as is ETG. All modes are stable in the barrier region. The plasma core is found to have no well resolved, strongly unstable plasma modes.

b) Growth rates (~10^6/sec) from linear calculations for $k_\theta \rho_i$ from 0.1 to 0.8, the ITG-TEM range of wave vectors, exhibits the well known parabolic ITG dependence on wave vector, when displayed on a linear plot.

Figure 6. Normalized driving forces for drift mode microturbulence are balanced to stabilize instabilities inside and at the ITB, compared to outside the ITB. Calculations were fully electromagnetic and included nonadiabatic electron response. Greatest destabilizing ITG-TEM plasma response occurs with increases in $-a_{ref} \nabla T_e/T_e$.

Figure 7. a) In the barrier region ITG-TEM is linearly destabilized as $-a_{ref} \nabla n_e/n_e$ is decreased. The experimental error bars are ~10%, with the experimental value of $-a_{ref} \nabla n_e/n_e$ being 0.60, far above the critical gradient destabilization point.

b) In the barrier region ITG-TEM is linearly destabilized as $-a_{ref} \nabla T_e/T_e$ is increased. The experimental error bars are ~10%, with the experimental value of $-a_{ref} \nabla T_e/T_e$ being 2.0, very close to marginal stability.

Figure 8. Comparison of microturbulence levels is shown by displaying the volume-integrated magnitude of the square of the fluctuation potential from nonlinear calculations in the three plasma regions at the trigger time. Nonlinear electrostatic simulations of C-Mod before the ITB show the linear phase, followed by saturation. At the ITB region, the square of the fluctuation potential is reduced by two orders of magnitude, and by one order of magnitude in the plasma core, compared to the ITG-TEM unstable region outside the plasma core. A GAM (a device size

and temperature dependent numerical mode) develops in the plasma core. The linear conclusion, that microturbulence is quiescent in the barrier region at this time, is also found in the nonlinear simulations.

Figure 9. Nonlinear results in the plasma core

a) Quasineutrality maintained in the plasma core to less than 1%.

b) The particle flux is outward, with electron and deuterium fluxes of similar magnitude and boron flux negligible.

c) The heat flux is outward, with the deuterium heat flux being greater than the electron heat flux. The boron carries negligible heat flux.

Figure 10. Nonlinear results in the transport barrier region

a) Quasineutrality maintained in the plasma ITB region to much less than 1%.

b) The particle flux from electrons and deuterium is inward, with electron and deuterium fluxes of similar magnitude and boron flux being very small. c) The heat flux is outward, with the deuterium heat flux being about twice the electron heat flux. The boron carries negligible heat flux.

Figure 11. Nonlinear results outside the ITB region

a) Quasineutrality maintained outside the ITB region to ~1%.

b) The particle flux is inward, with electron flux ~30% greater than the deuterium flux and boron flux negligible.

c) The heat flux is outward, with the deuterium heat flux being about five times the electron heat flux. The boron carries negligible heat flux.

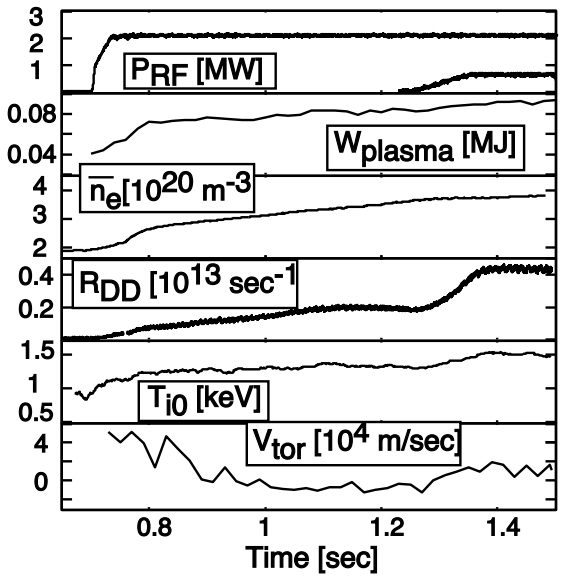
3
2
1
P_RF [MW]
0.08
0.04
W_plasma [MJ]
4
3
2
n_e [10^20 m^-3]
0.4
0.2
R_DD [10^13 sec^-1]
1.5
1
0.5
T_i0 [keV]
4
0
V_tor [10^4 m/sec]
0.8
1
1.2
1.4
Time [sec]

Fig 1

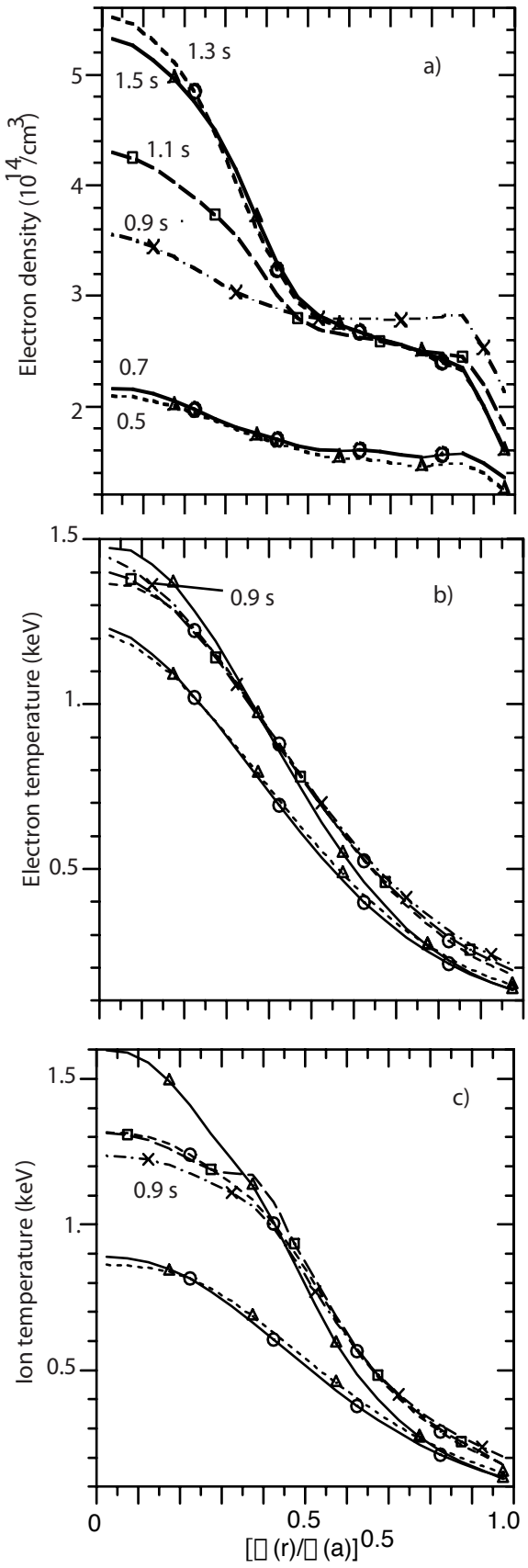
a)
1.3 s
1.5 s
1.1 s
0.9 s
0.7
0.5
Electron density (10^{14}/cm^3)
b)
0.9 s
Electron temperature (keV)
c)
0.9 s
Ion temperature (keV)
[□(r)/□(a)]$^{0.5}$

Fig. 2

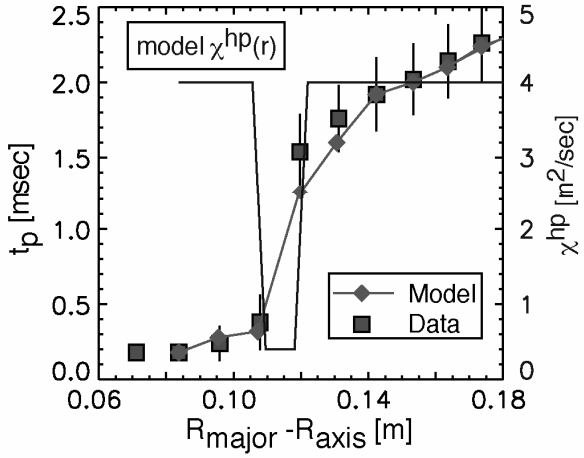
model $\chi^{hp}(r)$
Model
Data
t_p [msec]
χ^{hp} [m^2/sec]
R_{major} -R_{axis} [m]
0.0
0.5
1.0
1.5
2.0
2.5
0
1
2
3
4
5
0.06
0.10
0.14
0.18

Fig 3

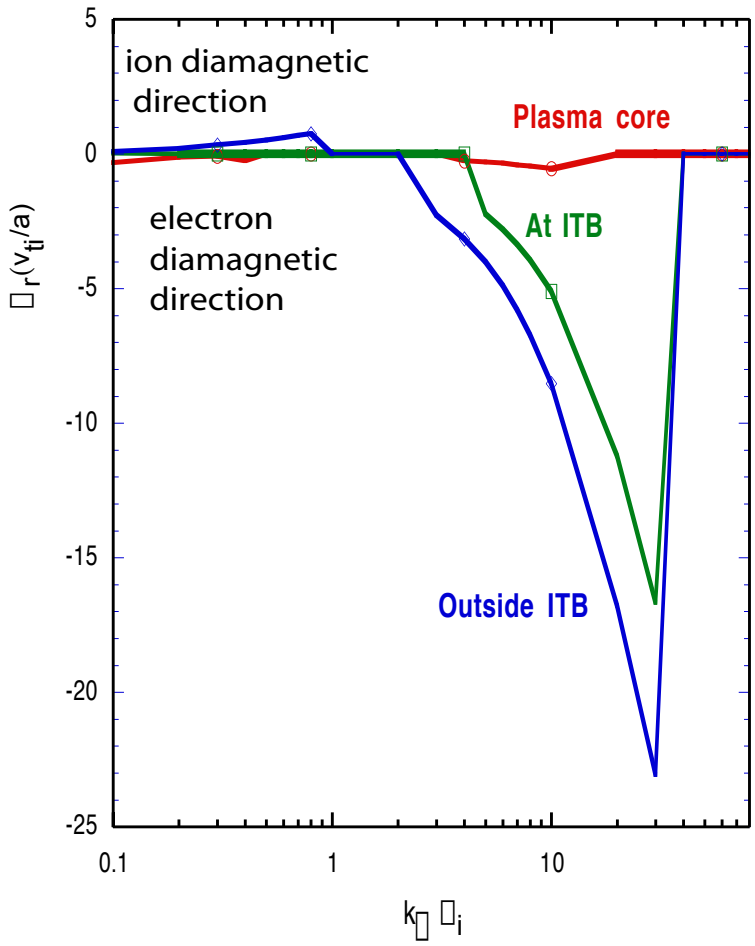
ion diamagnetic
direction
Plasma core
At ITB
electron
diamagnetic
direction
Outside ITB
5
0
-5
-10
-15
-20
-25
0.1
1
10

Fig 4

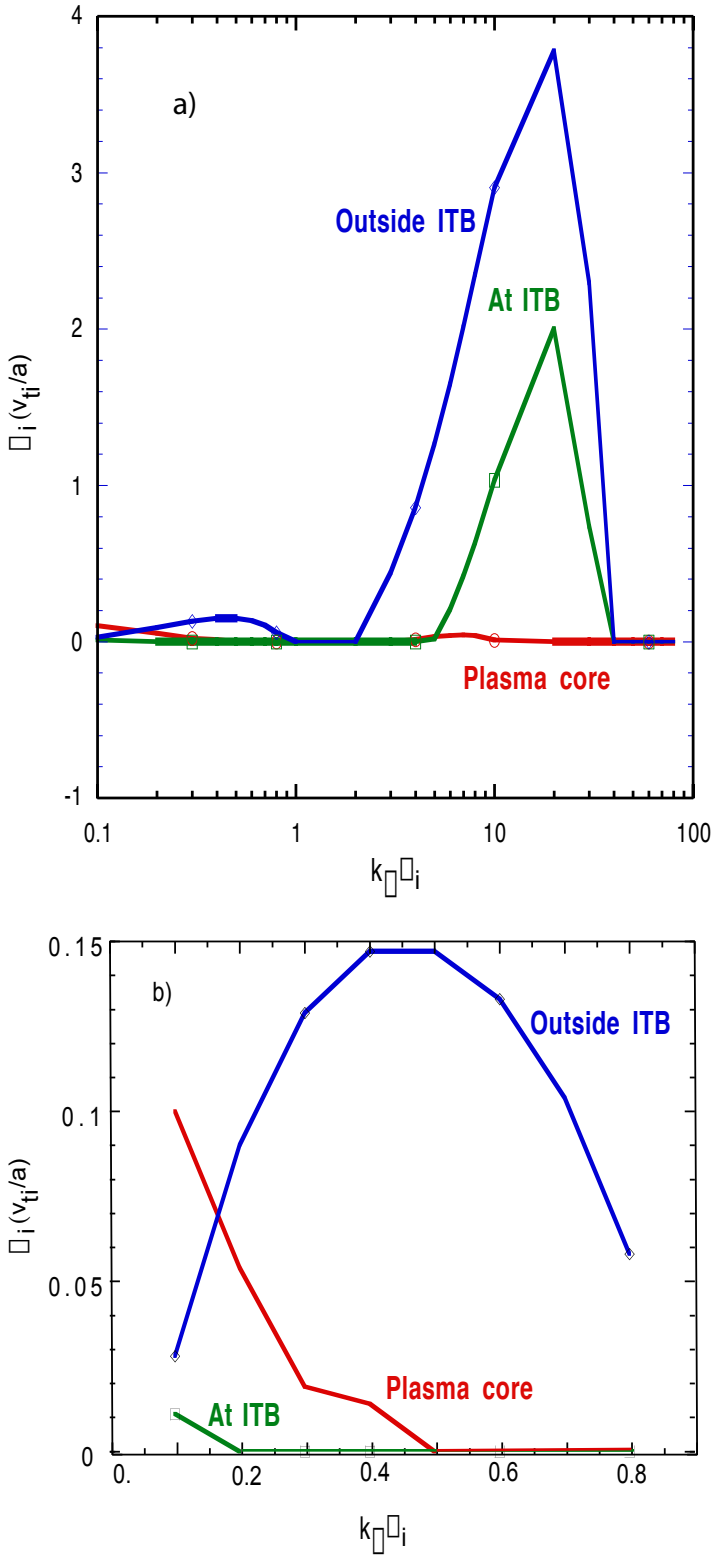
a)
Outside ITB
At ITB
Plasma core
4
3
2
1
0
-1
0.1
1
10
100
b)
Outside ITB
Plasma core
At ITB
0.15
0.1
0.05
0
0.
0.2
0.4
0.6
0.8

Fig 5

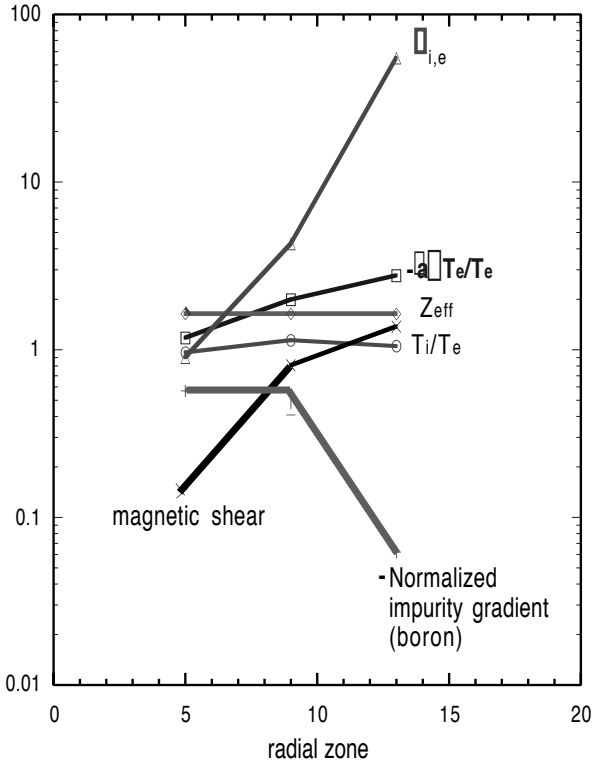
100
10
1
0.1
0.01
0
5
10
15
20
radial zone
i,e
Te/Te
Zeff
Ti/Te
magnetic shear
Normalized
impurity gradient
(boron)

Fig 6

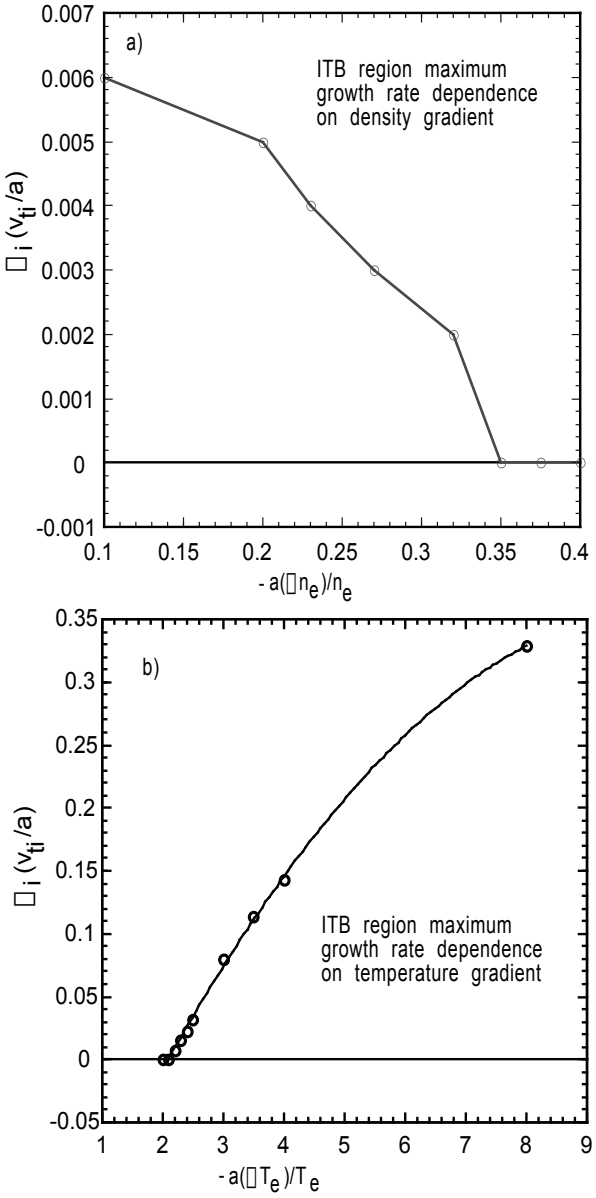
a)
ITB region maximum
growth rate dependence
on density gradient
0.007
0.006
0.005
0.004
0.003
0.002
0.001
0
-0.001
0.1
0.15
0.2
0.25
0.3
0.35
0.4
- a(∇n_e)/n_e
b)
ITB region maximum
growth rate dependence
on temperature gradient
0.35
0.3
0.25
0.2
0.15
0.1
0.05
0
-0.05
1
2
3
4
5
6
7
8
9
- a(∇T_e)/T_e

Fig 7

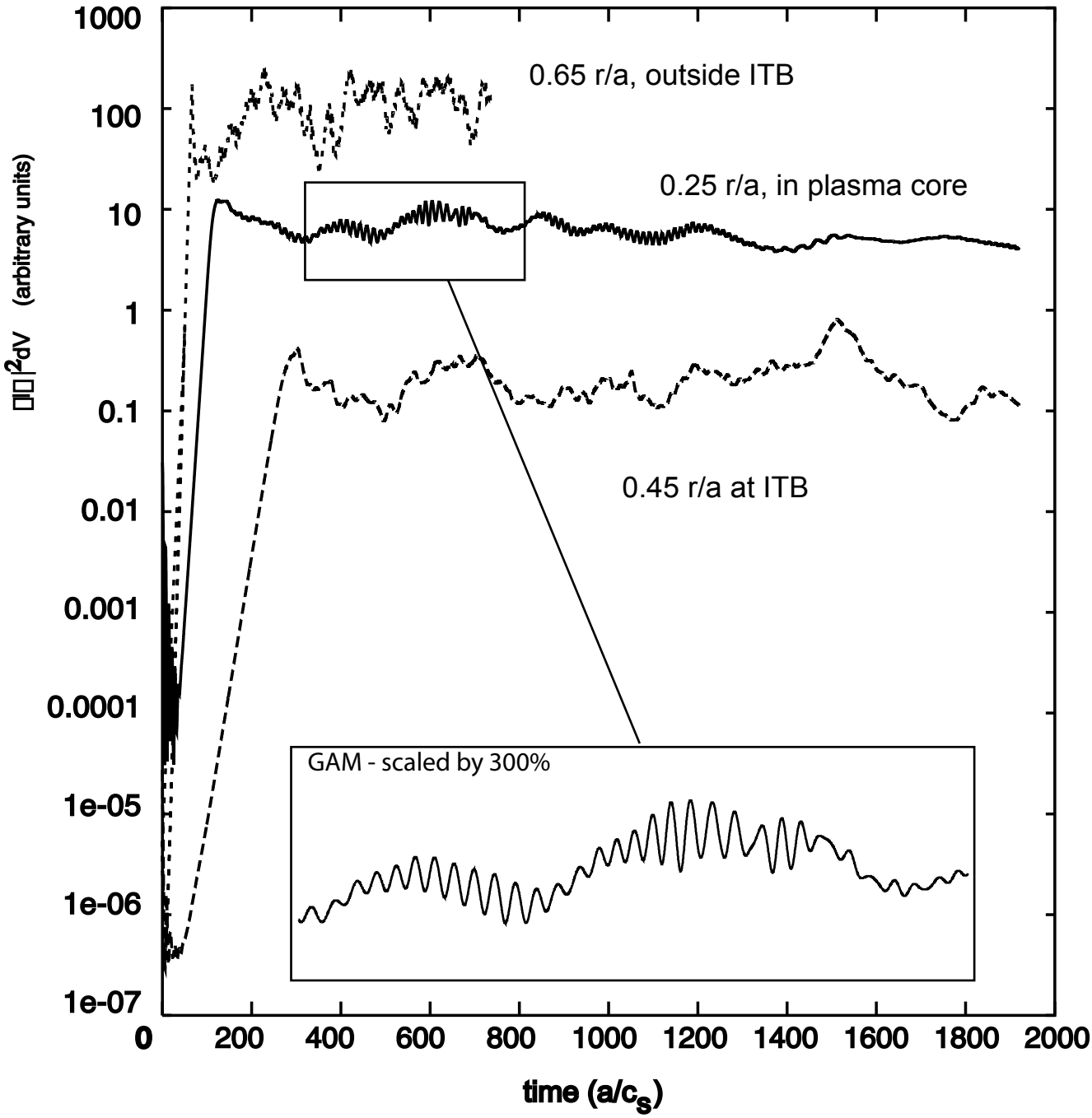
0.65 r/a, outside ITB
0.25 r/a, in plasma core
0.45 r/a at ITB
GAM - scaled by 300%
(arbitrary units)
time (a/c_s)
1000
100
10
1
0.1
0.01
0.001
0.0001
1e-05
1e-06
1e-07
0
200
400
600
800
1000
1200
1400
1600
1800
2000

Redi, Fig. 8

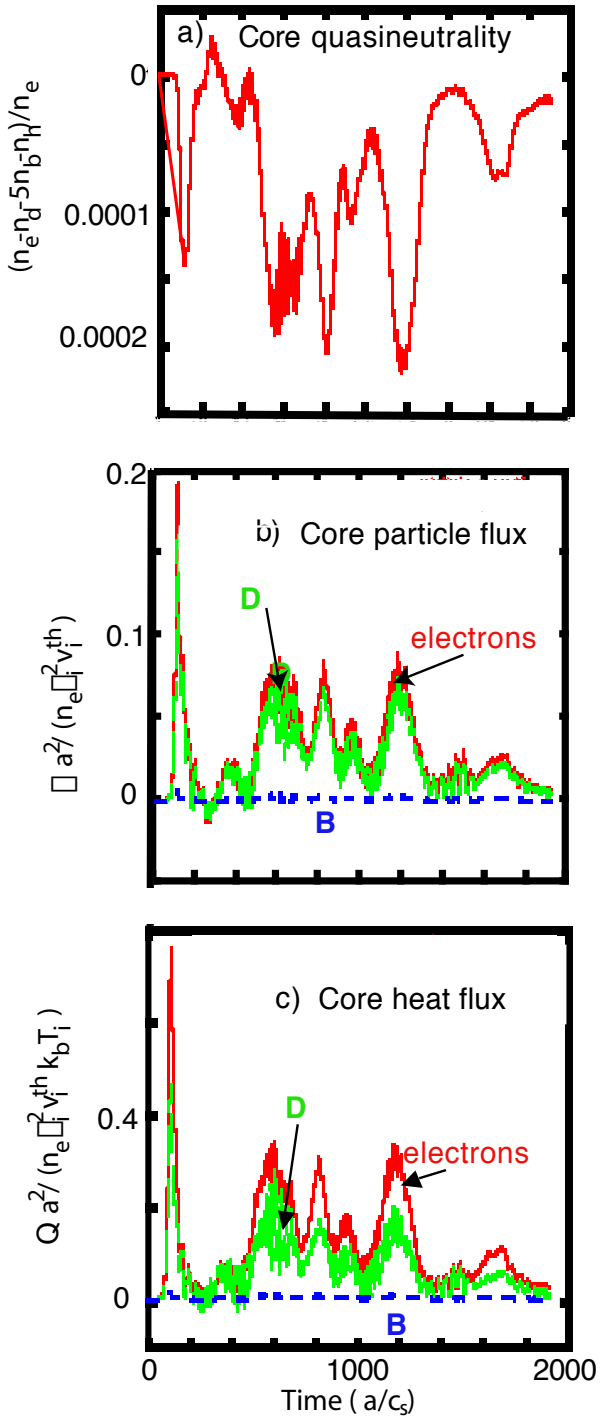
a) Core quasineutrality
$(n_e-n_d-5n_i-n_H)/n_e$
0
0.0001
0.0002
b) Core particle flux
$\Gamma a^2/(n_e L_T v_i^{th})$
0.2
0.1
0
D
electrons
B
c) Core heat flux
$Q a^2/(n_e L_T v_i^{th} k_b T_i)$
0.4
0
D
electrons
B
0
1000
2000
Time (a/c_s)

Fig 9

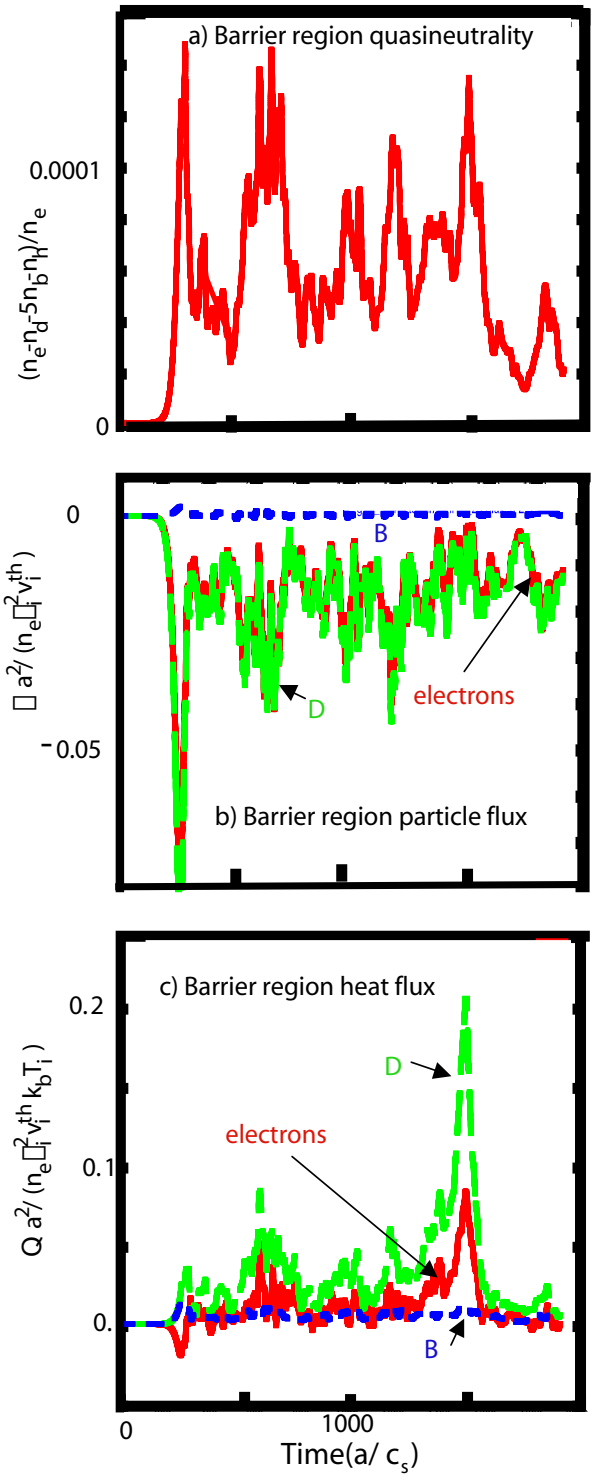
a) Barrier region quasineutrality
0.0001
0
$(n_e-n_d-5n_b-n_H)/n_e$
0
B
D
electrons
-0.05
b) Barrier region particle flux
c) Barrier region heat flux
0.2
D
electrons
0.1
0.
B
0
1000
Time(a/ c_s)

Fig 10

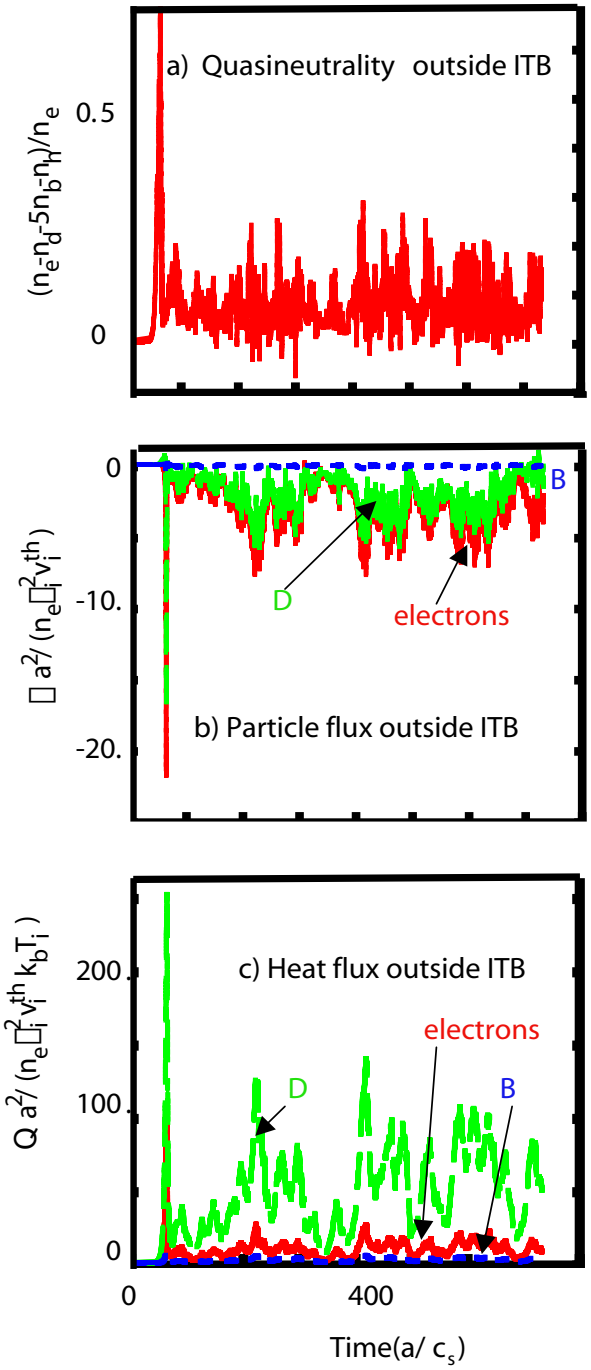
a) Quasineutrality outside ITB
0.5
0
b) Particle flux outside ITB
0
-10.
-20.
B
D
electrons
c) Heat flux outside ITB
200
100
0
electrons
D
B
0
400
Time(a/ c_s)

Fig11